

Charged kaon production in tau decays at LEP

DELPHI Collaboration

P. Abreu^t, W. Adam^g, T. Adye^{ak}, E. Agasi^{ad}, I. Ajinenko^{ap}, R. Aleksan^{am}, G.D. Alekseevⁿ, P.P. Allport^u, S. Almedhed^w, F.M.L. Almeida^{au}, S.J. Alvsvaag^d, U. Amaldi^g, A. Andreazza^{aa}, P. Antilogus^x, W.-D. Apel^o, R.J. Apsimon^{ak}, Y. Arnoud^{am}, B. Åsman^{ar}, J.-E. Augustin^r, A. Augustinus^{ad}, P. Baillon^g, P. Bambade^r, F. Barao^t, R. Barate^l, G. Barbiellini^{at}, D.Y. Bardinⁿ, G.J. Barker^{ah}, A. Baroncelli^{an}, O. Barring^g, J.A. Barrio^y, W. Bartl^{ay}, M.J. Bates^{ak}, M. Battaglia^m, M. Baubillier^v, J. Baudot^{am}, K.-H. Becks^{ba}, M. Begalli^{aj}, P. Beilliere^f, P. Beltranⁱ, A.C. Benvenuti^e, M. Berggren^{ao}, D. Bertrand^b, F. Bianchi^{as}, M. Bigi^{as}, M.S. Bilenkyⁿ, P. Billoir^v, J. Bjarne^w, D. Bloch^h, J. Blocki^{az}, S. Blyth^{ah}, V. Bocci^{al}, P.N. Bogolubovⁿ, T. Bolognese^{am}, M. Bonesini^{aa}, W. Bonivento^{aa}, P.S.L. Booth^u, G. Borisov^{ap}, C. Bosio^{an}, B. Bostjancic^{aq}, S. Bosworth^{ah}, O. Botner^{av}, B. Bouquet^r, C. Bourdarios^r, T.J.V. Bowcock^u, M. Bozzo^k, S. Braibant^b, P. Branchini^{an}, K.D. Brand^{ai}, R.A. Brenner^m, H. Briand^v, C. Bricman^b, L. Brillault^v, R.C.A. Brown^g, P. Bruckman^p, J.-M. Brunet^f, L. Bugge^{af}, T. Buran^{af}, A. Buys^g, J.A.M.A. Buytaert^g, M. Caccia^{aa}, M. Calvi^{aa}, A.J. Camacho Rozas^{ao}, R. Campion^u, T. Camporesi^g, V. Canale^{al}, K. Cankocak^{ar}, F. Cao^b, F. Carena^g, P. Carrilho^{au}, L. Carroll^u, R. Cases^{aw}, C. Caso^k, M.V. Castillo Gimenez^{aw}, A. Cattai^g, F.R. Cavallo^e, L. Cerrito^{al}, V. Chabaud^g, A. Chan^a, Ph. Charpentier^g, J. Chauveau^v, P. Checchia^{ai}, G.A. Chelkovⁿ, P. Chliapnikov^{ap}, V. Chorowicz^v, J.T.M. Chrin^{aw}, V. Cindro^{aq}, P. Collins^{ah}, J.L. Contreras^r, R. Contri^k, E. Cortina^{aw}, G. Cosme^r, F. Couchot^r, H.B. Crawley^a, D. Crennell^{ak}, G. Crosetti^k, J. Cuevas Maestro^{ag}, S. Czellar^m, E. Dahl-Jensen^{ab}, J. Dahm^{ba}, B. Dalmagne^r, M. Dam^{af}, G. Damgaard^{ab}, E. Daubie^b, A. Daum^o, P.D. Dauncey^{ak}, M. Davenport^g, J. Davies^u, W. Da Silva^v, C. Defoix^f, P. Delpierre^z, N. Demaria^{ah}, A. De Angelis^g, H. De Boeck^b, W. De Boer^o, S. De Brabandere^b, C. De Clercq^b, M.D.M. De Fez Laso^{aw}, C. De La Vaissiere^v, B. De Lotto^{at}, A. De Min^{aa}, L. De Paula^{au}, C. De Saint-Jean^{am}, H. Dijkstra^g, L. Di Ciaccio^{al}, F. Djama^h, J. Dolbeau^f, M. Donszelmann^g, K. Doroba^{az}, M. Dracos^h, J. Drees^{ba}, M. Dris^{ae}, Y. Dufour^g, F. Dupont^l, D. Edsall^a, R. Ehret^o, T. Ekelof^{av}, G. Ekspong^{ar}, M. Elsing^{ba}, J.-P. Engel^h, N. Ershaidat^v, M. Espirito Santo^t, D. Fassouliotis^{ae}, M. Feindt^g, A. Fenyuk^{ap}, A. Ferrer^{aw}, T.A. Filippas^{ae}, A. Firestone^a, H. Foeth^g, E. Fokitis^{ae}, F. Fontanelli^k, F. Formenti^g, J.-L. Fousset^z, S. Francon^x, B. Franek^{ak}, P. Frenkiel^f, D.C. Fries^o, A.G. Frodesen^d, R. Fruhwirth^{ay}, F. Fulda-Quenzer^r, H. Furstenau^g, J. Fuster^g, D. Gamba^{as},

M. Gandelman^q, C. Garcia^{aw}, J. Garcia^{ao}, C. Gaspar^g, U. Gasparini^{ai}, Ph. Gavillet^g,
 E.N. Gazis^{ae}, D. Gele^h, J-P. Gerber^h, L. Gerdyukov^{ap}, P. Giacomelli^g, D. Gillespie^g,
 R. Gokieli^{az}, B. Golob^{aq}, V.M. Golovatyukⁿ, J.J. Gomez Y Cadenas^g, G. Gopal^{ak}, L. Gorn^a,
 M. Gorski^{az}, V. Gracco^k, F. Grard^b, E. Graziani^{an}, G. Grosdidier^r, P. Gunnarsson^{ar}, J. Guy^{ak},
 U. Haedinger^o, F. Hahn^{ba}, M. Hahn^{ar}, S. Hahn^{ba}, S. Haider^{ad}, Z. Hajduk^p, A. Hakansson^w,
 A. Hallgren^{av}, K. Hamacher^{ba}, W. Hao^{ad}, F.J. Harris^{ah}, V. Hedberg^w, R. Henriques^t,
 J.J. Hernandez^{aw}, J.A. Hernando^{aw}, P. Herquet^b, H. Herr^g, T.L. Hessing^u, E. Higon^{aw},
 H.J. Hilke^g, T.S. Hill^a, S-O. Holmgren^{ar}, P.J. Holt^{ah}, D. Holthuizen^{ad}, P.F. Honore^f,
 M. Houlden^u, J. Hrubec^{ay}, K. Huet^b, K. Hultqvist^{ar}, P. Ioannou^c, P-S. Iversen^d,
 J.N. Jackson^u, R. Jacobsson^{ar}, P. Jalocha^p, G. Jarlskog^w, P. Jarry^{am}, B. Jean-Marie^r,
 E.K. Johansson^{ar}, M. Jonker^g, L. Jonsson^w, P. Juillot^h, M. Kaiser^o, G. Kalmus^{ak},
 F. Kapusta^v, M. Karlsson^{ar}, E. Karvelasⁱ, S. Katsanevas^c, E.C. Katsoufis^{ae}, R. Keranen^g,
 B.A. Khomenkoⁿ, N.N. Khovanskiⁿ, B. King^u, N.J. Kjaer^{ab}, H. Klein^g, A. Klovning^d,
 P. Kluit^{ad}, A. Koch-Mehrin^{ba}, J.H. Koehne^o, B. Koene^{ad}, P. Kokkiniasⁱ, M. Koratzinos^{af},
 A.V. Korytovⁿ, V. Kostioukhine^{ap}, C. Kourkoumelis^c, O. Kouznetsovⁿ, P.H. Kramer^{ba},
 M. Krammer^{ay}, C. Kreuter^o, J. Krolikowski^{az}, I. Kronkvist^w, W. Krupinski^p, W. Kucewicz^p,
 K. Kulka^{av}, K. Kurvinen^m, C. Lacasta^{aw}, C. Lambropoulosⁱ, J.W. Lamsa^a, L. Lancieri^{at},
 P. Langefeld^{ba}, V. Lapin^{ap}, I. Last^u, J-P. Laugier^{am}, R. Lauhakangas^m, F. Ledroit^l,
 R. Leitner^{ac}, Y. Lemoigne^{am}, J. Lemonne^b, G. Lenzen^{ba}, V. Lepeltier^r, T. Lesiak^{ai},
 J.M. Levy^h, E. Lieb^{ba}, D. Liko^{ay}, R. Lindner^{ba}, A. Lipniacka^r, I. Lippi^{ai}, B. Loerstad^w,
 M. Lokajicek^j, J.G. Loken^{ah}, A. Lopez-Fernandez^g, M.A. Lopez Aguera^{ao}, M. Los^{ad},
 D. Loukasⁱ, J.J. Lozano^{aw}, P. Lutz^{am}, L. Lyons^{ah}, G. Maehlum^o, J. Maillard^f, A. Maio^t,
 A. Maltezosⁱ, F. Mandl^{ay}, J. Marco^{ao}, B. Marechal^{au}, M. Margoni^{ai}, J-C. Marin^g,
 C. Mariotti^{an}, A. Markouⁱ, T. Maron^{ba}, S. Marti^{aw}, C. Martinez-Rivero^{ao}, F. Martinez-Vidal^{aw},
 F. Matorras^{ao}, C. Matteuzzi^{aa}, G. Matthiae^{al}, M. Mazzucato^{ai}, M. Mc Cubbin^u, R. Mc Kay^a,
 R. Mc Nulty^u, J. Medbo^{av}, C. Meroni^{aa}, W.T. Meyer^a, M. Michelotto^{ai}, E. Migliore^{as},
 I. Mikulec^{ay}, L. Mirabito^x, W.A. Mitaroff^{ay}, G.V. Mitselmakherⁿ, U. Mjoernmark^w,
 T. Moa^{ar}, R. Moeller^{ab}, K. Moenig^g, M.R. Monge^k, P. Morettini^k, H. Mueller^o,
 W.J. Murray^{ak}, B. Muryn^p, G. Myatt^{ah}, F. Naraghi^l, F.L. Navarra^e, P. Negri^{aa}, S. Nemecek^j,
 W. Neumann^{ba}, N. Neumeister^{ay}, R. Nicolaidou^c, B.S. Nielsen^{ab}, P. Niss^{ar}, A. Nomerotski^{ai},
 A. Normand^{ah}, M. Novak^j, V. Obraztsov^{ap}, A.G. Olshevskiⁿ, R. Orava^m, K. Osterberg^m,
 A. Ouraou^{am}, P. Paganini^r, M. Paganoni^{aa}, R. Pain^v, H. Palka^p, Th.D. Papadopoulou^{ae},
 L. Pape^g, F. Parodi^k, A. Passeri^{an}, M. Pegoraro^{ai}, J. Pennanen^m, L. Peralta^t, H. Pernegger^{ay},
 M. Pernicka^{ay}, A. Perrotta^c, C. Petridou^{at}, A. Petrolini^k, H.T. Phillips^{ak}, G. Piana^k,
 F. Pierre^{am}, M. Pimenta^t, S. Plaszczynski^r, O. Podobrin^o, M.E. Pol^q, G. Polok^p, P. Poropat^{at},
 V. Pozdniakovⁿ, M. Prest^{at}, P. Privitera^{al}, A. Pullia^{aa}, D. Radojicic^{ah}, S. Ragazzi^{aa},
 H. Rahmani^{ae}, P.N. Ratoff^s, A.L. Read^{af}, M. Reale^{ba}, P. Rebecchi^r, N.G. Redaelli^{aa},
 M. Regler^{ay}, D. Reid^g, P.B. Renton^{ah}, L.K. Resvanis^c, F. Richard^r, J. Richardson^u, J. Ridky^j,
 G. Rinaudo^{as}, I. Ripp^{am}, A. Romero^{as}, I. Roncagliolo^k, P. Ronchese^{ai}, V. Ronjin^{ap}, L. Roos^l,
 E.I. Rosenberg^a, E. Rosso^g, P. Roudeau^r, T. Rovelli^e, W. Ruckstuhl^{ad},

V. Ruhlmann-Kleider^{am}, A. Ruiz^{ao}, A. Rybin^{ap}, H. Saarikko^m, Y. Sacquin^{am}, G. Sajot^{el},
 J. Salt^{aw}, J. Sanchez^y, M. Sannino^k, S. Schael^g, H. Schneider^o, M.A.E. Schyns^{ba},
 G. Sciolla^{as}, F. Scuri^{at}, A.M. Segar^{ah}, A. Seitz^o, R. Sekulin^{ak}, M. Sessa^{at}, R. Seufert^o,
 R.C. Shellard^{aj}, I. Siccama^{ad}, P. Siegrist^{am}, S. Simonetti^{am}, F. Simonetto^{ai}, A.N. Sisakianⁿ,
 T.B. Skaali^{af}, G. Smadja^x, O. Smirnovaⁿ, G.R. Smith^{ak}, R. Sosnowski^{az}, D. Souza-Santos^{aj},
 T. Spassov^t, E. Spiriti^{an}, S. Squarcia^k, H. Staeck^{ba}, C. Stanescu^{an}, S. Stapnes^{af}, I. Stavitski^{ai},
 G. Stavropoulosⁱ, K. Stepaniak^{az}, F. Stichelbaut^g, A. Stocchi^r, J. Strauss^{ay}, J. Straver^g,
 R. Strub^h, B. Stugu^d, M. Szczekowski^{az}, M. Szeptycka^{az}, T. Tabarelli^{aa}, O. Tchikilev^{ap},
 G.E. Theodosiou^l, Z. Thome^{au}, A. Tilquin^z, J. Timmermans^{ad}, V.G. Timofeevⁿ,
 L.G. Tkatchevⁿ, T. Todorov^h, D.Z. Toet^{ad}, A. Tomaradze^b, B. Tome^t, E. Torassa^{as},
 L. Tortora^{an}, G. Transtromer^w, D. Treille^g, W. Trischuk^g, G. Tristram^f, C. Troncon^{aa},
 A. Tsirou^g, E.N. Tsyganovⁿ, M-L. Turluer^{am}, T. Tuuva^m, I.A. Tyapkin^v, M. Tyndel^{ak},
 S. Tzamarias^u, B. Ueberschaer^{ba}, S. Ueberschaer^{ba}, O. Ullaland^g, V. Uvarov^{ap}, G. Valenti^e,
 E. Vallazza^g, J.A. Valls Ferrer^{aw}, C. Vander Velde^b, G.W. Van Apeldoorn^{ad}, P. Van Dam^{ad},
 M. Van Der Heijden^{ad}, W.K. Van Doninck^b, J. Van Eldik^{ad}, P. Vaz^g, G. Vegni^{aa}, L. Ventura^{ai},
 W. Venus^{ak}, F. Verbeure^b, M. Verlato^{ai}, L.S. Vertogradovⁿ, D. Vilanova^{am}, P. Vincent^x,
 L. Vitale^{at}, E. Vlasov^{ap}, A.S. Vodopyanovⁿ, M. Vollmer^{ba}, M. Voutilainen^m, V. Vrba^j,
 H. Wahlen^{ba}, C. Walck^{ar}, F. Waldner^{at}, A. Wehr^{ba}, M. Weierstall^{ba}, P. Weilhammer^g,
 A.M. Wetherell^g, J.H. Wickens^b, M. Wielers^o, G.R. Wilkinson^{ah}, W.S.C. Williams^{ah},
 M. Winter^h, M. Witek^g, G. Wormser^r, K. Woschnagg^{av}, K. Yip^{ah}, O. Yushchenko^{ap},
 A. Zaitsev^{ap}, A. Zalewska^p, P. Zalewski^{az}, D. Zavrtanik^{aq}, E. Zevgolatakos^l, N.I. Ziminⁿ,
 M. Zito^{am}, D. Zontar^{aq}, R. Zuberi^{ah}, G. Zumerle^{ai}

^a Ames Laboratory and Department of Physics, Iowa State University, Ames IA 50011, USA

^b Physics Department, Univ. Instelling Antwerpen, Universiteitsplein 1, B-2610 Wilrijk, Belgium
 and IIHE, ULB-VUB, Pleinlaan 2, B-1050 Brussels, Belgium

and Faculté des Sciences, Univ de l'Etat Mons, Av. Maistriau 19, B-7000 Mons, Belgium

^c Physics Laboratory, University of Athens, Solonos Str 104, GR-10680 Athens, Greece

^d Department of Physics, University of Bergen, Allégaten 55, N-5007 Bergen, Norway

^e Dipartimento di Fisica, Università di Bologna and INFN, Via Irnerio 46, I-40126 Bologna, Italy

^f Collège de France, Lab de Physique Corpusculaire, IN2P3-CNRS, F-75231 Paris Cedex 05, France
^g CERN, CH-1211 Geneva 23, Switzerland

^h Centre de Recherche Nucléaire, IN2P3 - CNRS/ULP - BP20, F-67037 Strasbourg Cedex, France

ⁱ Institute of Nuclear Physics, N C S R Demokritos, P.O. Box 60228, GR-15310 Athens, Greece

^j FZU, Inst of Physics of the C A S. High Energy Physics Division, Na Slovance 2, 180 40, Praha 8, Czech Republic

^k Dipartimento di Fisica, Università di Genova and INFN, Via Dodecaneso 33, I-16146 Genova, Italy

^l Institut des Sciences Nucléaires, IN2P3-CNRS, Université de Grenoble 1, F-38026 Grenoble Cedex, France

^m Research Institute for High Energy Physics, SEFT, P.O. Box 9, FIN-00014 Helsinki, Finland

ⁿ Joint Institute for Nuclear Research, Dubna, Head Post Office, P.O. Box 79, 101 000 Moscow, Russian Federation

^o Institut für Experimentelle Kernphysik, Universität Karlsruhe, Postfach 6980, D-76128 Karlsruhe, Germany

^p High Energy Physics Laboratory, Institute of Nuclear Physics, Ul. Kawory 26a, PL-30055 Krakow 30, Poland

^q Centro Brasileiro de Pesquisas Físicas, rua Xavier Sigaud 150, BR-22290 Rio de Janeiro, Brazil

^r Université de Paris-Sud, Lab de l'Accélérateur Linéaire, IN2P3-CNRS, Bat 200, F-91405 Orsay Cedex, France

^s School of Physics and Materials, University of Lancaster, Lancaster LA1 4YB, UK

^t LIP, IST, FCUL - Av. Elias Garcia, 14-1(o), P-1000 Lisboa Codex, Portugal

^u Department of Physics, University of Liverpool, P.O. Box 147, Liverpool L69 3BX, UK

^v LPNHE, IN2P3-CNRS, Universités Paris VI et VII, Tour 33 (RdC), 4 place Jussieu, F-75252 Paris Cedex 05, France

^w Department of Physics, University of Lund, Sölvegatan 14, S-22363 Lund, Sweden

- ^x *Université Claude Bernard de Lyon, IPNL, IN2P3-CNRS, F-69622 Villeurbanne Cedex, France*
^y *Universidad Complutense, Avda. Complutense s/n, E-28040 Madrid, Spain*
^z *Univ d'Aix - Marseille II - CPP, IN2P3-CNRS, F-13288 Marseille Cedex 09, France*
^{aa} *Dipartimento di Fisica, Università di Milano and INFN, Via Celoria 16, I-20133 Milan, Italy*
^{ab} *Niels Bohr Institute, Blegdamsvej 17, DK-2100 Copenhagen 0, Denmark*
^{ac} *NC, Nuclear Centre of MFF, Charles University, Areal MFF, V Holesovickach 2, 180 00, Praha 8, Czech Republic*
^{ad} *NIKHEF-H, Postbus 41882, NL-1009 DB Amsterdam, The Netherlands*
^{ae} *National Technical University, Physics Department, Zografou Campus, GR-15773 Athens, Greece*
^{af} *Physics Department, University of Oslo, Blindern, N-1000 Oslo 3, Norway*
^{ag} *Dpto Fisica, Univ Oviedo, C/P Jimenez Casas, S/N-33006 Oviedo, Spain*
^{ah} *Department of Physics, University of Oxford, Keble Road, Oxford OX1 3RH, UK*
^{ai} *Dipartimento di Fisica, Università di Padova and INFN, Via Marzolo 8, I-35131 Padova, Italy*
^{aj} *Depto. de Fisica, Pontificia Univ Católica, C.P. 38071 RJ-22453 Rio de Janeiro, Brazil*
^{ak} *Rutherford Appleton Laboratory, Chilton, Didcot OX11 0QX, UK*
^{al} *Dipartimento di Fisica, Università di Roma II and INFN, Tor Vergata, I-00173 Rome, Italy*
^{am} *Centre d'Etude de Saclay, DSM/DAPNIA, F-91191 Gif-sur-Yvette Cedex, France*
^{an} *Istituto Superiore di Sanità, Ist Naz di Fisica Nucl (INFN), Viale Regina Elena 299, I-00161 Rome, Italy*
^{ao} *C.E.A F.M., C.S.I.C. - Univ Cantabria, Avda los Castros, (CICYT-AEN93-0832), S/N-39006 Santander, Spain*
^{ap} *Inst. for High Energy Physics, Serpukov P.O. Box 35, Protvino, (Moscow Region), Russian Federation*
^{aq} *J Stefan Institute and Department of Physics, University of Ljubljana, Jamova 39, SI-61000 Ljubljana, Slovenia*
^{ar} *Fysikum, Stockholm University, Box 6730, S-113 85 Stockholm, Sweden*
^{as} *Dipartimento di Fisica Sperimentale, Università di Torino and INFN, Via P. Giuria 1, I-10125 Turin, Italy*
^{at} *Dipartimento di Fisica, Università di Trieste and INFN, Via A. Valerio 2, I-34127 Trieste, Italy*
^{au} *and Istituto di Fisica, Università di Udine, I-33100 Udine, Italy*
^{av} *Univ Federal do Rio de Janeiro, C.P. 68528 Cidade Univ, Ilha do Fundão BR-21945-970 Rio de Janeiro, Brazil*
^{aw} *Department of Radiation Sciences, University of Uppsala, P.O. Box 535, S-751 21 Uppsala, Sweden*
^{ax} *IFIC, Valencia-CSIC, and D.F.A.M.N., U. de Valencia, Avda. Dr. Moliner 50, E-46100 Burjassot (Valencia), Spain*
^{ay} *Institut für Hochenergiephysik, Österr Akad. d. Wissensch, Nikolsdorfergasse 18, A-1050 Vienna, Austria*
^{az} *Inst Nuclear Studies and University of Warsaw, Ul Hoza 69, PL-00681 Warsaw, Poland*
^{ba} *Fachbereich Physik, University of Wuppertal, Postfach 100 127, D-42097 Wuppertal 1, Germany*

Received 17 June 1994

Editor: L. Montanet

Abstract

Kaon production in one prong tau decays has been studied using data collected with the DELPHI detector at the LEP collider. Charged kaons were identified over a large momentum range by the DELPHI barrel Ring Imaging Cherenkov detector. The following branching ratios have been determined: $\text{BR}(\tau \rightarrow K\nu_\tau) = (0.85 \pm 0.18)\%$, $\text{BR}(\tau \rightarrow K\nu_\tau \geq 0 \text{ neutrals}) = (1.54 \pm 0.24)\%$, $\text{BR}(\tau \rightarrow K\nu_\tau \geq 1 \text{ neutrals}) = (0.69 \pm 0.25)\%$. The result for the exclusive branching ratio is consistent with the Standard Model prediction based on $\tau - \mu - e$ universality. In addition, tau decay into K^{*-} was studied in the channel $K^{*-} \rightarrow K^-\pi^0$. The result $\text{BR}(\tau \rightarrow K^{*-}\nu_\tau) \times \text{BR}(K^{*-} \rightarrow K^-\pi^0) = (0.57 \pm 0.23)\%$ was obtained.

1. Introduction

Kaon production in single prong τ decays has been measured using a data sample corresponding to 392 000 hadronic Z^0 events recorded with the DELPHI detector at LEP in 1992. The τ decays involving kaons probe the W coupling to the weak hadronic current. While these decays are strongly suppressed

by the Cabibbo angle in weak interactions, this is generally not expected for new superweak interactions. The branching ratio $\text{BR}(\tau \rightarrow K\nu_\tau)$ would be sensitive to extensions of the Standard Model that violate lepton universality.

The present measurements exploit the charged kaon identification capability of the Ring Imaging Cherenkov (RICH) detector over a large momentum

range. The exclusive decay rate $\tau \rightarrow K\nu_\tau$ was measured by tagging events with well identified isolated kaons, and the high granularity of the electromagnetic calorimeter was then used to reject decays with neutral pions in the final state. The inclusive kaon production $\tau \rightarrow K\nu_\tau \geq 0$ neutrals was measured by separating kaons on a statistical basis from pions and muons.

After a short description of the DELPHI detector in Section 2, and of the event selection in Section 3, the performance of the RICH detector and the procedure for kaon identification are discussed in Section 4. Section 5 reports the analysis of the exclusive decay channel. The measurement of the kaon fraction in inclusive τ decays and the determination of inclusive branching ratios from these data are described in Section 6. Finally, the results are discussed and summarized in Section 7.

2. The DELPHI detector

The DELPHI detector has been described in detail elsewhere [1]. In the barrel region, charged particle tracks were reconstructed by a set of cylindrical tracking detectors whose axes are parallel to the 1.23 T solenoidal magnetic field and to the beam direction. The Time Projection Chamber (TPC) is the device providing the main tracking information. Track segments closer to the beam pipe were measured by the Inner Detector (ID), which is a cylindrical drift chamber, and by the microvertex detector (VD), which consists of three concentric layers of silicon microstrip detectors located between the beam pipe and the ID. The barrel Ring Imaging Cherenkov (barrel RICH) detector surrounds the TPC. Track measurements outside the barrel RICH were provided by the Outer Detector (OD), located between the barrel RICH and the electromagnetic calorimeter. The momentum resolution was measured to be $\sigma_p/p = 0.0008 \times p(\text{GeV}/c)$.

The charged hadrons are identified by the Cherenkov angle measurement in the barrel RICH detector [2], which covers polar angles to the electron beam direction, θ , between 40° and 140° . A support wall divides the 3.5 m long cylindrical detector into two halves. Each side is subdivided into 12 azimuthal sectors. A sector contains two adjacent 1 cm thick C_6F_{14} liquid radiators, 12 cm in front of a pair of drift tubes. The 40 cm deep gas radiator volume behind

the drift tubes is filled with C_5F_{12} . Sets of parabolic mirrors (six per drift tube) focus Cherenkov photons from the gas radiator onto the drift tubes. The projection has the form of a ring with a diameter proportional to the Cherenkov angle. In the drift tubes, photons of wavelengths between 160 and 220 nm are converted into electrons by a photosensitive gas additive, TMAE (Tetrakis diMethyl Amino Ethylene). These photo-electrons are drifted towards a multiwire proportional chamber (MWPC) whose signals define the location of the photon conversion points with an accuracy of about 1 mm in all directions. Almost all particles passing through the radiators also traverse a drift tube. This leads to large ionization signals, since the MWPCs were operated at high gain for efficient single photo-electron detection.

Electromagnetic showers were reconstructed in the High Density Projection Chamber (HPC) in the barrel region. This detector covers the polar angular range between 41° and 139° . The gas sampling technique used in the HPC provides a three-dimensional charge distribution measurement with high granularity. The energy resolution was studied using electromagnetic showers from Bhabha events, Compton electrons and $\mu^+\mu^-\gamma$ radiative events. The measured energy resolution for photons of energy E is $\sigma_E/E = 0.29/\sqrt{E(\text{GeV})} \oplus 0.04$.

Muon identification was based on the barrel Muon Chambers consisting of two layers of drift tubes, the first one inside, the second outside the hadron calorimeter, which surrounds the coil of the magnet.

3. Event selection

The sample of $Z^0 \rightarrow \tau^+\tau^-$ candidates was selected by requiring a single particle in one hemisphere, and up to five particles in the opposite hemisphere. Hemispheres were defined by the plane perpendicular to the event thrust axis. Only charged particles with momenta larger than $0.2 \text{ GeV}/c$, with a distance of closest approach to the interaction region less than 1.5 cm in the plane perpendicular to the beam and less than 4.5 cm along the beam direction, were considered. Events were accepted if one of the single prong tracks was within a polar angle acceptance of $45^\circ < \theta < 135^\circ$ where θ is the polar angle to the electron beam direction.

For the inclusive measurement, the event selection was similar to that of Ref. [3]. The isolation angle, defined as the angle between the single prong particle and the nearest particle in the opposite hemisphere, was required to be greater than 160° . This condition rejected most of the hadronic events. The two-photon background was suppressed by requiring at least 8 GeV of visible energy and a total event transverse momentum larger than $0.4 \text{ GeV}/c$. The $Z^0 \rightarrow \mu^+\mu^-$ and $Z^0 \rightarrow e^+e^-$ background was removed by the following three cuts. The acollinearity between the two jets was required to be greater than 0.5° . The electron pair background was suppressed by requiring the quantity $\sqrt{E_1^2 + E_2^2}$ to be less than E_{beam} , where E_1 and E_2 are the electromagnetic energy in a 30° cone around the thrust axis in each hemisphere and E_{beam} is the beam energy. The muon pair background was suppressed by requiring the corresponding momentum variable $\sqrt{p_1^2 + p_2^2}$ to be less than E_{beam}/c , where p_1 and p_2 are the momenta of the most energetic particles in each hemisphere. From a detailed simulation of the detector and using the KORALZ event generator [4], the efficiency of this selection of τ pairs inside the acceptance was measured to be $(81.6 \pm 0.7)\%$ with a background of $(1.9 \pm 0.4)\%$ from other Z^0 decays.

For the exclusive measurement, the event selection was adapted to the kinematical conditions for kaon identification in the RICH. As explained in the following section, kaons in the fiducial volume of the barrel RICH with momentum between $4 \text{ GeV}/c$ and $20 \text{ GeV}/c$ can be identified unambiguously. The first step in the event selection was to require a single charged particle meeting these conditions. This already resulted in a clean sample of $\tau^+\tau^-$ events, since Z^0 decays into $\mu^+\mu^-$ and e^+e^- were rejected by the upper momentum cut at $20 \text{ GeV}/c$, and Z^0 hadronic decays by the requirement of only one charged particle in one hemisphere. The minimal momentum of $4 \text{ GeV}/c$ effectively reduces the number of two-photon events in the sample. In order to reject remaining hadronic and two-photon events, it was required that the number of charged particles in the opposite hemisphere be at most three, with at least a total momentum of $1 \text{ GeV}/c$. Further, the isolation angle was required to be larger than 165° . Events were rejected when more than 1 GeV energy from charged particles plus electromagnetic showers was observed outside a cone of 25° around the thrust axis.

The final step in the exclusive event selection was to remove τ decays with electrons or π^0 's in the final state, using the total energy deposit in the electromagnetic calorimeter. A single prong candidate was rejected if it met any of the following criteria:

- The energy and the longitudinal profile of the shower in the HPC associated with the track were consistent with the electron hypothesis.
- The total electromagnetic energy in a cone of 25° around the thrust axis was larger than the momentum of the single prong track.
- The neutral electromagnetic energy E_N in the decay was higher than 1 GeV, where E_N was the summed energy of all showers in the 25° cone excluding the shower associated to the track.

The efficiency for passing the event selection cuts was 91.4% for τ decays into π or K , where the hadron meets the kinematical and geometrical conditions for particle identification in the barrel RICH.

The composition of the exclusive event sample was studied by comparing it with a corresponding sample of KORALZ [4] simulated events. No significant differences were found. The main contribution to the selected sample of single prong decays comes from the decay $\tau \rightarrow \mu\nu_\mu\nu_\tau$ where $(64.5 \pm 1.8)\%$ of the tracks were identified as muons, by using the muon chambers, in data and $(66.3 \pm 0.6)\%$ in Monte Carlo. The charged multiplicity N_c in the unbiased opposite hemisphere was checked. The background sources lead either to $N_c = 1$ (leptonic Z^0 decays, two-photon events, cosmics) or to high multiplicities (hadronic Z^0 decays). The observed fractions of events with $N_c = 2$ and 3 agree with the expectation from pure τ decays within the statistical errors of 1%. From these comparisons it is concluded that the composition of the final sample is reproduced by the $\tau^+\tau^-$ Monte Carlo simulation to better than 2%.

4. Kaon identification and performance of the RICH detector

Kaons produced in τ decays at the Z^0 energy have momenta above $3.5 \text{ GeV}/c$. The Cherenkov angle in the liquid radiator is already saturated at its maximum value in this momentum region. Therefore, only the data from the gas radiator are used.

Two different techniques were used for kaon iden-

tification in the gas radiator. Between 4 GeV/ c and ~ 9 GeV/ c , kaons were below the threshold for producing Cherenkov photons, while pions and muons yield nearly saturated angles. In this momentum range kaons were identified by “veto identification”, i.e. by requiring that no photo-electrons were associated to the particle. Below 4 GeV/ c the Cherenkov angle for pions and the number of radiated photons decreases, and no attempt was made to identify kaons. Above the kaon threshold of ~ 9 GeV/ c the Cherenkov angle was determined from the detected Cherenkov photons. This is called “ring identification” and, as explained below, it allows kaon identification up to 20 GeV/ c . Together the two kaon identification methods cover a large part of the phase space available in τ decays at LEP.

Cuts were developed to ensure that only tracks with reliable RICH and tracking information would be included in the analysis. These cuts were studied with muons from $Z^0 \rightarrow \mu^+ \mu^-$ events, electrons from $Z^0 \rightarrow e^+ e^-$ events, and selected tracks from single prong τ decays. Tracks had to be contained in the fully efficient fiducial volume of the RICH: $47^\circ < \theta < 86^\circ$ and $94^\circ < \theta < 133^\circ$. The region around the midwall at 90° had a reduced efficiency and was therefore cut out.

The location and the direction of a particle passing through the radiator were used to calculate the corresponding Cherenkov angle from the measured position of each detected photon. Tracking a particle through the RICH radiator was done by interpolation between the track elements measured in the TPC and in the Outer Detector. In the inclusive measurement 15% of the candidate tracks were rejected because the track fit had less than 40 degrees of freedom or a χ^2 per degree of freedom greater than three. On average, a track had 51 degrees of freedom. Less stringent cuts for the exclusive measurement rejected 5% of the tracks. The resolution σ_γ on the angle of a single photo-electron depends on the parameters of the track and on the position of the photo-electron in the RICH detector [2]. It was measured with dimuon events and was found to be 4.5 mrad on average, consistent with expectation. The saturated Cherenkov angle in the gas $\theta_{(\pi,\mu)}$ was found to be 61 mrad and this value was constant through the entire data taking period.

Veto identification

In the veto identification region it is important to ensure on a track-by-track basis that the RICH is fully active. For this reason at least three ionization hits were required along the particle track in the drift tube. With this requirement about 12% of the tracks were lost. This loss was mainly due to a longitudinal gap between adjacent drift tubes. A particle passing through one of these gaps cannot produce ionization electrons, although the focussing mirrors guarantee full efficiency for detection of Cherenkov photons for these tracks.

For reliable veto identification the yield of photo-electrons had to be well understood. The number of associated photo-electrons was defined as the number of detected photo-electrons in a window around $\theta_{(\pi,\mu)}$ of width $\pm 2.5\sigma_\gamma$ ($\pm 5.0\sigma_\gamma$) in the exclusive (inclusive) measurement. The expected number of photo-electrons was calculated for each track [2]. It depends on the mass and the momentum of the particle and its position in the RICH, since the length of radiator traversed by a particle increases with decreasing polar angle. The distribution of the number n of photo-electrons per track in dimuon events is shown in Fig. 1a. It has a mean value of 7.9. The measured and expected photo-electron distributions are in good agreement. This includes the bin with zero photo-electrons, which was used for the veto identification. In Figs. 1b and 1c the same distributions are shown for tracks from single prong τ decays. In Fig. 1b the particles have momenta between 20 GeV/ c and 35 GeV/ c , where the mean expected number of photo-electrons is near its saturation value for all particles. Fig. 1c shows the distribution for particles selected for the exclusive analysis with momenta in the veto identification region. Here the expected number of photo-electrons was normalized to particles with observed photo-electrons. Almost all particles without photo-electrons are expected to be kaons with momenta below the Cherenkov threshold. The distribution of observed photo-electrons was identical, within statistical errors, for the three samples. The momentum dependence of the observed number of photons was studied on muons and pions from one prong τ decays and was found to be in agreement with expectation.

Since in veto mode a particle was identified as a kaon if no associated photo-electrons were observed, the misidentification rate was the probability

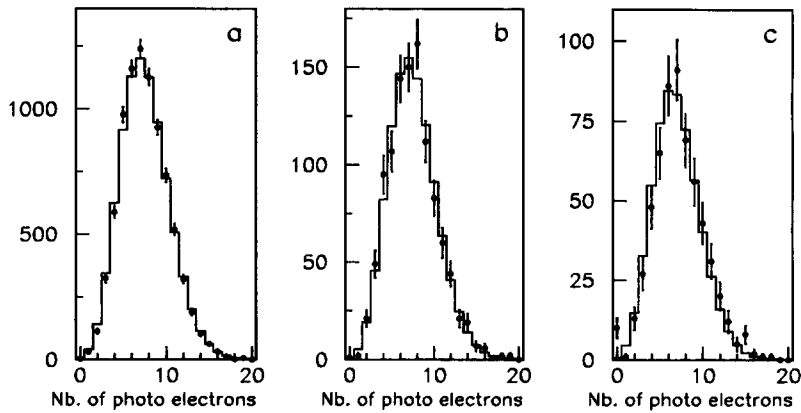


Fig. 1 Observed and expected number of photo-electrons per particle: (a) $Z \rightarrow \mu^+ \mu^-$ events; (b) high momentum particles from single prong τ decay, (c) particles from single prong τ decay in the veto region of kaon identification. The expected distribution (c) is for muons and pions only. The observed excess in the data at zero photo-electrons is due to kaons.

of observing no photo-electrons for a muon or pion. From dimuon events and high momentum particles, the misidentification rates were found to be compatible with Poisson statistics for the expected number of photo-electrons. It was estimated for each track, taking into account the slight decrease of the number of photo-electrons at low momentum. The result was $(0.15 \pm 0.04)\%$ for the exclusive sample, and $(0.25 \pm 0.09)\%$ in the inclusive analysis. This higher value is due to the remaining electron tracks and interacting hadrons in the inclusive sample.

The inefficiency for kaon identification in veto mode was given by the probability of finding a noise hit in the window around $\theta_{(\pi, \mu)}$. This probability was calculated from the final samples of kaon candidates in veto identification. All photo-electrons were counted in the large area corresponding to 120 mrad around the tracks where the pattern recognition program searches for photon candidates. From scaling of the areas it was concluded that the efficiency for kaon veto identification is larger than 99% and $(98 \pm 1)\%$ in the exclusive and inclusive measurements, respectively.

Ring identification

Kaons with momenta above the threshold of ~ 9 GeV/c and up to 20 GeV/c were identified by measuring the Cherenkov angle. For the determination of the average Cherenkov angle θ_c for each track, the detected photo-electrons were grouped into clusters of similar angle. For each cluster an angle θ_c was cal-

culated as the weighted average of all photo-electrons in the cluster, with a weight equal to $1/\sigma_\gamma^2$. Photo-electrons with an individual Cherenkov angle within a $\pm 2.5 \sigma_\gamma$ window around θ_c were kept in the cluster. A cluster had to contain at least two photo-electrons. An iterative procedure used the $\pm 2.5 \sigma_\gamma$ criterion to remove background hits and to allow inclusion of new photo-electrons into the clusters. The probability that the photons belong to the same ring was determined using the expected errors σ_γ . If the probability was less than 3% the procedure for dropping background hits was started again. Only tracks with one final cluster were kept for the analysis. Tracks with more than 35% of the photo-electrons in the bands between $2.5 \sigma_\gamma$ and $5.0 \sigma_\gamma$ above and below the mean value were excluded. The efficiency of the procedure was studied with a dedicated simulation program and with muon candidates from one prong τ decays. Simulation and data showed good agreement both in the asymptotic value of the efficiency and in its momentum behaviour near threshold. For tracks well above threshold, an efficiency of 91% was thus determined for the procedure of Cherenkov angle determination in the inclusive measurement. An efficiency of 96% was obtained for the exclusive analysis, as the fact that π^0 s have been removed allows the cuts on the ring probability to be avoided. Fig. 2 shows the measured Cherenkov angle as a function of particle momentum for the data sample used in the inclusive study. Also shown are the expected angles for K and (π, μ) . A

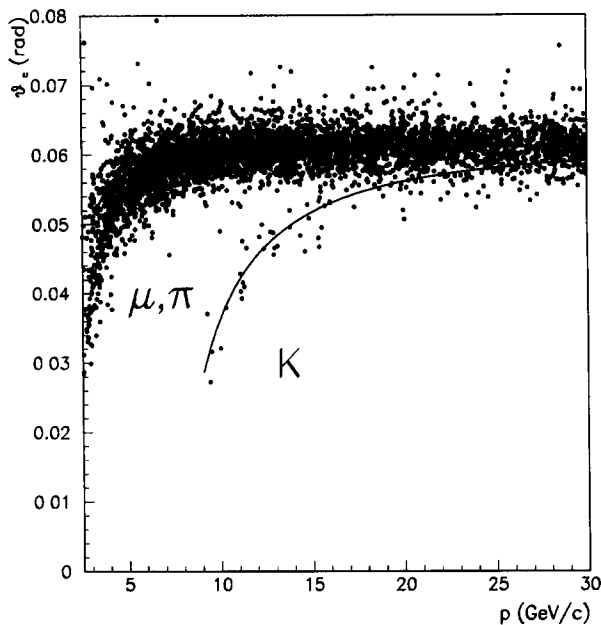


Fig. 2 Measured Cherenkov angle versus momentum for single prong τ decays. The expected angle for K , π and μ are also shown

kaon population around the expected line is clearly observed.

From the errors σ_γ of the individual photo-electrons, the expected value σ_θ of the uncertainty on θ_c was calculated. It varied from track to track between 0.5 mrad and 4 mrad, with an average of 1.6 mrad. This variation was mainly due to statistical fluctuations in the number of photo-electrons. The resolution function of θ_c , defined as the difference between the measured and the expected Cherenkov angle divided by the expected error, is shown for $Z^0 \rightarrow \mu^+\mu^-$ events in Fig. 3. The distribution is well described by a fit to the sum of two Gaussian distributions. The main Gaussian had a standard deviation of 1.01, indicating that in most cases the measured Cherenkov angle agrees with the expected value within the calculated error, independent of the number of observed photons. The tails in the distribution are mainly due to background photo-electrons and misalignments of mirrors; they were accounted for with a second Gaussian with a relative amplitude of 0.10 and standard deviation of 1.96.

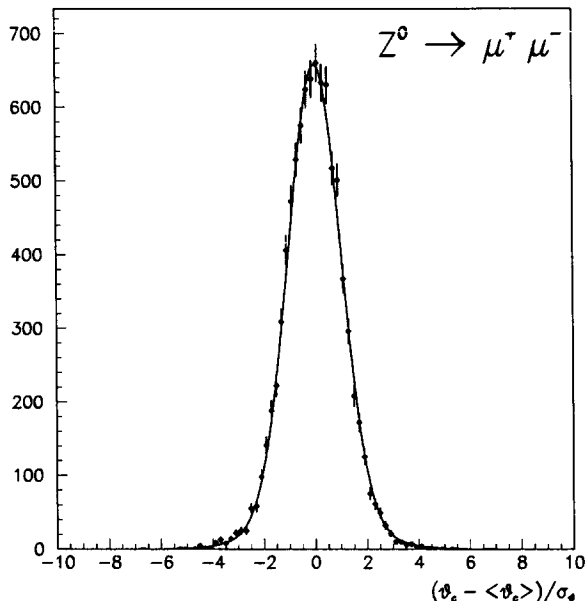


Fig. 3 Distribution of the difference between the measured and expected Cherenkov angle for $Z \rightarrow \mu^+\mu^-$ events, in units of the expected error. The solid line is the result of a two-Gaussian fit described in the text.

5. Measurement of the branching ratio $\tau \rightarrow K\nu_\tau$

In this section an analysis is described which was optimized for the exclusive decay $\tau \rightarrow K\nu_\tau$. Due to the low branching ratio the measurement was limited by the available statistics. Therefore, a high efficiency was important, and a specially adapted event selection was used. Kaons were tagged on a track by track basis in conditions where their RICH response was well separated from the pion response. The cuts were optimized to minimize the systematic effects in kaon identification, most of which cancel in the ratio of kaons to (π, μ) .

A particle was identified as a kaon in veto mode, or in ring mode if the measured Cherenkov angle was compatible with the kaon hypothesis within $\pm 2.5 \sigma_\theta$ and incompatible with the (π, μ) hypothesis, i.e. more than $n_{\text{sep}} \sigma_\theta$ below $\theta_{(\pi, \mu)}$. From the resolution function of the Cherenkov angle (Fig. 3) the value $n_{\text{sep}} = 4.0$ was chosen. Similarly, a particle was accepted in the (π, μ) class if the observed Cherenkov angle was compatible with $\theta_{(\pi, \mu)}$ and incompatible with the expected kaon angle θ_K . Using these cuts the identification efficiency was similar for both classes.

The efficiency for particle identification at the four standard deviation level was around 83 to 91% for momenta ranging from 4 to 15 GeV/c. A 5% inefficiency due to track quality cuts and a geometrical inefficiency of 12% for the detection of ionization signals in veto identification have been discussed in Section 4. In ring identification 4% of the particles were rejected because the Cherenkov angle was not well determined. At momenta above 15 GeV/c the bands around the K and the (π, μ) hypotheses overlap, and the separation cut rejected an increasing number of tracks. At 20 GeV/c good $K - \pi$ separation on a track by track basis was still possible for $\sim 10\%$ of the cases. Just above the kaon threshold both veto and ring identification were used. In this momentum region, a kaon radiates a small number of photons allowing the Cherenkov angle to be measured. In addition, this angle is small and no photon was emitted in the $2.5 \sigma_\gamma$ band around $\theta_{(\pi, \mu)}$. Therefore, the kaon would also be properly identified in veto mode. Although both methods could be applied in this region, neither was fully efficient. The inefficiencies of the two methods were complementary and the efficiency for particle identification had no gap in the transition region between the two methods. The systematic uncertainty in the identification efficiency due to the low photon yield of kaons near threshold was estimated to be 0.3%.

The kaon fraction in the single prong τ sample was calculated from the number of events with an unambiguously identified kaon, relative to the number of events in the (π, μ) class. The branching ratio of the decay $\tau \rightarrow K\nu_\tau$ was obtained from this measured fraction and from the results of the Monte Carlo simulation. The different steps are outlined in Table 1. The first line gives the number of kaon candidates. The analysis was repeated for the veto and ring methods separately. Since both methods were applied to particles between about 8 GeV/c and 10 GeV/c, the splitting of the samples was done on a statistical basis. For this reason, the number of observed particles in the K and (π, μ) class are not integers.

The misidentification probability and inefficiency in veto mode were discussed in Section 4. The ring identification depends critically on the resolution function, shown in Fig. 3. The method of individually tagging kaons to 4 standard deviations allows good control of the systematic uncertainties in the momentum region where the kaon band partially overlaps with the (π, μ)

one. These systematic effects were estimated from the sample itself. The misidentification probability was calculated by integrating the tails of the resolution function measured with dimuon events. To estimate the systematic uncertainties, the minimal separation $n_{\text{sep}} \sigma_\theta$ was varied. By increasing n_{sep} the background due to misidentification decreases, but the identification efficiency becomes lower. The $K/(\pi, \mu)$ ratio was stable within 2% for $n_{\text{sep}} \geq 4$, but starts to decrease at lower values, due to a difference in the tails of the resolution function between high momentum muons and particles from τ decay. In Table 1 a 2% relative systematic error on the number of identified kaons was used for the ring misidentification subtraction.

The number of background $\tau \rightarrow K^* \nu_\tau$ decays passing the cuts was taken from the simulation. Other decays to $K^* \pi$, $K^* K$ and KK^0 give a negligible contribution. The quoted uncertainty corresponds to twice the experimental error on the branching ratios [5] and amounts to 25% of the correction. The event selection described in Section 3 resulted in a non- τ background of less than 2%, however only about 2% of the charged particles in the sample were kaons. To exclude an unexpected accumulation of background, each of the 30 tagged kaon candidate events was inspected, paying special attention to the unbiased hemisphere opposite to the kaon. Kaons are frequently produced in two-photon events. Such events always contain two kaons with momenta below 20 GeV/c. In none of the candidate events was any particle in the opposite hemisphere compatible with the kaon hypothesis. The background from hadronic Z^0 decays was estimated by scaling the prediction of the JETSET Monte Carlo program [6] to the number of selected events with charged multiplicity $N_c=4$ and 5 that did not pass the HPC cuts. The probability to have a hadronic event in the kaon candidate sample was lower than 2% and was neglected.

The contribution from each τ decay mode to the (π, μ) class had to be known to calculate the branching ratio from the number of particles in the background subtracted K sample and in the (π, μ) class. The KORALZ [4] simulation was used to determine these contributions. The momentum dependent efficiency for RICH identification was applied to all particles in the simulated sample that passed the event selection cuts. This yielded a conversion factor $f = 2.39$ from the ratio of events to the branching ratio.

Table 1

Determination of BR ($\tau \rightarrow K\nu_\tau$). In the lower part, the systematic errors are listed (see text).

	Combined	Veto	Ring
<i>K</i> Candidates	30 00 ± 5.48	10.15 ± 3.19	19.85 ± 4.46
Misidentifications	2 04 ± 0.42	0 80 ± 0.23	1 24 ± 0.35
<i>K</i> * Background	1.22 ± 0 31	0 17 ± 0 04	1.06 ± 0 26
<i>K</i> Signal	26 74 ± 5 49	9.18 ± 3.19	17.56 ± 4.48
(π, μ) Signal	1316.	555 20	760 80
Sample Composition	± 0 017	± 0 017	± 0 017
Efficiency	± 0.005	± 0.007	± 0.003
Asymm. Resolution	± 0.027		± 0.047
BR ($\tau \rightarrow K\nu_\tau$) [%]	0 85 ± 0 18	0 73 ± 0 25	0.94 ± 0.25

The remaining systematic uncertainties in the measured branching ratio due to kaon identification and other sources are listed in the lower part of Table 1. They were much smaller than the statistical ones, since most effects cancel in the ratio of kaons to (π, μ). As stated in Section 3, the uncertainty on the conversion factor *f* due to the sample composition was found to be 2%. The uncertainty on the veto identification efficiency was found in Section 4 to be 1% and it was seen above that it was 0.3% for the ring identification efficiency.

The largest systematic error in ring identification arises from the asymmetry of the resolution function. More background photo-electrons are detected on the outside of the Cherenkov ring than on the inside because of the increased area. The measured Cherenkov angle was therefore slightly biased towards large values. As a consequence the identification efficiencies for kaons and (π, μ) tracks were different. The requirement of good separation between kaons and pions rejects a fraction of the tracks in the momentum region where the bands of Cherenkov angles for kaons and pions partially overlap. For the rejected kaons the measured Cherenkov angle was larger than the expected one, whereas for the rejected pions it was smaller. The bias introduced by this effect was estimated from the data in a special analysis to be 5%, which was taken as the systematic error. It was small compared to the statistical errors, since in exclusive τ decays the photo-electron background is low. For comparison, the bias caused by the asymmetry was <1% for dimuon tracks, where the background was lower.

The branching ratio determined from the selected

kaon sample is

$$\text{BR}(\tau \rightarrow K\nu_\tau) = (0.85 \pm 0.18)\%,$$

where the error includes the statistical error and the systematic uncertainties listed in Table 1. As can be seen in Table 1, it is in good agreement with the branching ratios from the veto and ring methods separately.

6. Inclusive kaon production

The kaon fraction in inclusive one prong τ decays was measured in the veto identification region from 4.0 to 9.0 GeV/*c*, and in the ring identification region from 9.0 to 20.0 GeV/*c*. These measurements were used to determine the inclusive branching ratio BR ($\tau \rightarrow K\nu_\tau \geq 0$ neutrals), and to extract the non-exclusive branching ratio BR ($\tau \rightarrow K\nu_\tau \geq 1$ neutrals) using the measurement of the exclusive branching ratio BR ($\tau \rightarrow K\nu_\tau$) reported in the previous section.

After applying the track and RICH quality cuts, τ decays into an electron were removed. Electrons were identified by combining the track and ionization energy loss measured in the TPC with the electromagnetic shower information from the HPC. The probability of the electron hypothesis was computed by comparing the track parameters and momentum with the shower position and energy, in combination with the measured ionization loss and the shower longitudinal development. This selected 1143 one prong τ candidates in the veto identification region between 4.0 and 9.0 GeV/*c*.

The fraction of tracks without associated Cherenkov photons was measured to be $(1.66 \pm 0.38)\%$ (19 events). From this number the misidentification rate of $(0.25 \pm 0.09)\%$ was subtracted, and the rate was corrected for the veto efficiency of $(98 \pm 1)\%$. The number of kaons, divided by the total number of tracks in the sample, was in this way measured to be:

$$R_{\text{veto}} = (1.45 \pm 0.40)\%,$$

where the error includes the statistical and the systematic uncertainties. Using the KORALZ [4] τ generator and passing the events through the full detector simulation, the relation between the measured quantity R_{veto} and the exclusive and non-exclusive branching ratios was determined to be:

$$R_{\text{veto}} = a_1 \text{BR}(\tau \rightarrow K\nu_\tau \geq 1 \text{ neutrals}) + a_2 \text{BR}(\tau \rightarrow K\nu_\tau), \quad (1)$$

with the kinematical factors $a_1 = 0.77 \pm 0.08$ and $a_2 = 1.14 \pm 0.09$, where the uncertainties were due to finite Monte Carlo statistics. The values of a_1 and a_2 reflect the different momentum spectra of the two decay modes.

Several additional sources of systematic uncertainty were investigated. The number of kaons from $q\bar{q}$ background was estimated using Monte Carlo simulation and normalized to the observed number of events passing all selections but the isolation criteria. This background gave a 3% error. Discrepancies between data and Monte Carlo for the rejection of electrons from τ decays introduced a 2% systematic error. The systematic error on the efficiency for kaon veto identification was 1%, as discussed in Section 4. Other systematic errors were negligible. The respective relative errors are given in Table 2.

The selected inclusive sample of one prong decays in the ring identification region of 9.0–20.0 GeV/ c contained 1815 tracks. The kaon content was obtained by fitting the percentage of kaon candidates in the sample. An unbinned Maximum Likelihood technique was used. This method is sensitive to the kaon contribution also in the kinematical region where there was partial overlap with the band of Cherenkov angles from lighter particles (see Fig. 2).

The likelihood function L per event was defined as follows:

Table 2

Summary of relative systematic errors on the measured rates R_{veto} and R_{ring}

Source	Veto	Ring
Background $q\bar{q} \rightarrow K$	0.03	0.01
Electron rejection	0.02	0.02
Efficiency	0.01	0.02
Parameterization	–	0.05
Total	0.04	0.06

$$L = \sum_{i=e,\mu,\pi,K} R_i \epsilon_i(p) S_i(p) F_i,$$

where R is the particle fraction, $\epsilon(p)$ the efficiency, $S(p)$ the momentum spectrum, and F the resolution function for the μ , π and K hypotheses and the remaining electrons. The likelihood function is normalized to one. The resolution function F was parameterized as a double Gaussian function with a mean value corresponding to the expected value for the Cherenkov angle θ_c for that hypothesis. The width of the Gaussians was based on the expected error on θ_c . The e , μ , π and K momentum spectra $S(p)$ were extracted from KORALZ [4] Monte Carlo including full detector simulation. The particle identification efficiency of the RICH as a function of momentum $\epsilon(p)$, was obtained from a dedicated Monte Carlo simulation. The fit had five free parameters: the kaon fraction R_K , the central value of the two Gaussian distributions, their amplitude ratio and two scaling terms for the width of the Gaussians. The fitting program was extensively tested on selected muon candidates and on simulated data. The systematic error on the kaon branching ratio due to uncertainties in the efficiency $\epsilon(p)$ was 2% (see Table 2).

The five parameter fit gave the following result for the inclusive fraction of kaons in the momentum range studied with ring identification:

$$R_{\text{ring}} \equiv R_K = (1.59 \pm 0.31)\%,$$

where the error includes the statistical and the systematic uncertainties. The result of the fit was found to be stable to variations of the momentum interval for the fit. As a further check, a one parameter fit was performed with the scaling parameters of the widths fixed at the values obtained from high momentum (20.0–30.0 GeV/ c) one prong τ events. The result of this fit

in the momentum region 9–20 GeV/c agreed within 2% with the result of the five parameter fit applied to the same momentum region, which demonstrates that the kaon fraction remained constant if the scaling parameters were determined in the high momentum region. As in the exclusive analysis, the largest systematic error was due to background photons which create an asymmetry between the tails of the distribution. This asymmetric resolution error on the quantity R_{ring} was obtained from detailed simulation and amounted to less than 5%. In Table 2 it was included in a total systematic error of 5% due to parameterization.

Using detector simulation as before, the measured quantity R_{ring} was related to the exclusive and non-exclusive branching ratios:

$$R_{\text{ring}} = b_1 \text{BR}(\tau \rightarrow K\nu_\tau \geq 1 \text{ neutrals}) + b_2 \text{BR}(\tau \rightarrow K\nu_\tau), \quad (2)$$

with $b_1 = 1.26 \pm 0.08$ and $b_2 = 0.84 \pm 0.04$, where the uncertainties were due to the finite statistics of the simulation.

The branching ratio $\text{BR}(\tau \rightarrow K\nu_\tau \geq 1 \text{ neutrals})$ was determined from Eqs. (1) and (2) by a simultaneous fit to the measured quantities $\text{BR}(\tau \rightarrow K\nu_\tau)$, R_{veto} and R_{ring} with proper account of their errors. The statistical errors on the coefficients a_1 , a_2 , b_1 and b_2 were taken into account in the fit. The quoted results assume that the kaon spectrum for $\tau \rightarrow K\nu_\tau \geq 1 \text{ neutrals}$ is given by the decay mode $\tau \rightarrow K^{*-}(892)\nu_\tau$. Decays proceeding through $K^*\pi$, K^*K and KK^0 lead to a softer kaon spectrum. No attempt was made to apply corrections for these decays. Their effect was propagated as an error into the fit result, assuming they contribute with a branching ratio of 0.21%, as obtained from the estimate below. It leads, for instance, to a systematic error of less than 3% on the inclusive branching ratio. Taking into account that, due to different selection criteria, 60% of the exclusive kaon sample was in common with the inclusive sample, the result of the fit was:

$$\text{BR}(\tau \rightarrow K\nu_\tau \geq 1 \text{ neutrals}) = (0.69 \pm 0.25)\%.$$

The statistical and systematic errors have been combined. The correlation coefficient with the exclusive branching ratio is -0.26 . The result for the inclusive measurement was:

Table 3
Relative systematic errors for the ratio of τ decay rates into $K^{*-}\nu_\tau$ and $\rho^-\nu_\tau$, with $K^{*-} \rightarrow K^-\pi^0$

Source	Error
M.C. statistics	0.07
Efficiency	0.02
Asymm resolution	0.10
π^0 reconstruction	0.05
Background $K^{*-} + \text{neutrals}$	0.10
Total	0.17

$$\text{BR}(\tau \rightarrow K\nu_\tau \geq 0 \text{ neutrals}) = (1.54 \pm 0.24)\%,$$

with a correlation coefficient with the exclusive branching ratio of 0.22.

Subtracting from $\text{BR}(\tau \rightarrow K\nu_\tau \geq 1 \text{ neutrals})$ the contribution from $K^{*-}(892)\nu_\tau$ with a branching ratio [5] of $(1.43 \pm 0.17)\%$, the remaining fraction of decay modes not proceeding through the $K^{*-}\nu_\tau$ mode is $\text{BR}_{\text{non } K^*\nu_\tau}(\tau \rightarrow K\nu_\tau \geq 1 \text{ neutrals}) = (0.21 \pm 0.26)\%$.

In addition, a measurement was made of the production rate of charged kaons in the decay $\tau \rightarrow K^{*-}\nu_\tau$, where $K^{*-} \rightarrow K^-\pi^0$. Kaon candidates were selected in both the veto and ring identification regions up to a momentum of 25 GeV/c. In the latter region kaons were individually tagged, similarly to the procedure described in Section 5 for the measurement of the branching ratio $\tau \rightarrow K\nu_\tau$, but with looser identification criteria: the Cherenkov angle was required to be within 2.5 times its error from the expected value for a kaon and to differ by more than 2 times its error from the value for a pion. The π^0 's were reconstructed either using one photon with an energy above 5 GeV, or using two photons both with an energy less than 10 GeV, having an invariant mass below 500 MeV/c² and an energy greater than 2 GeV similarly to Ref. [3]. No additional photon candidates were allowed in that hemisphere. The resulting $K^-\pi^0$ invariant mass distribution is shown in Fig. 4 and exhibits a clear peak at the expected K^{*-} mass position. The number of signal events was fitted to be 15 ± 5 events. The background is mainly due to pions that were misidentified as kaons.

Similarly, charged pions were selected and combined with a π^0 candidate to reconstruct ρ mesons. A total of 484 ± 36 ρ events was obtained. From

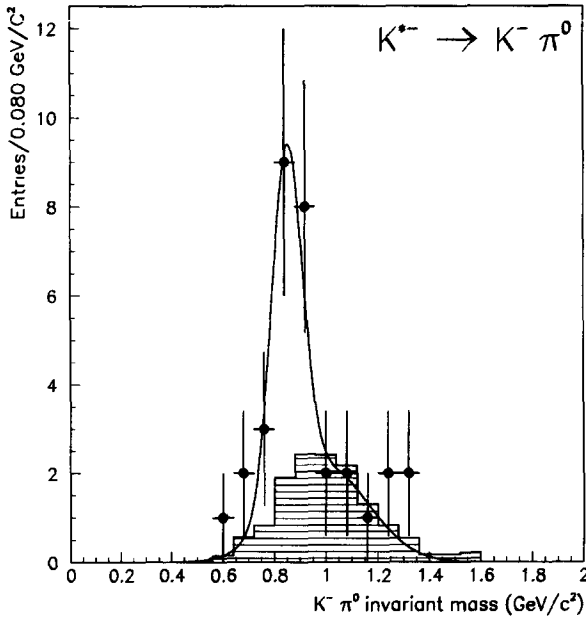


Fig 4 $K^-\pi^0$ invariant mass distribution with the fitted background from misidentified pions (hatched) and the K^{*-} signal plus background

these data the ratio $\text{BR}(\tau \rightarrow K^{*-}\nu_\tau) \times \text{BR}(K^{*-} \rightarrow K^-\pi^0) / \text{BR}(\tau \rightarrow \rho^-\nu_\tau)$ was determined. This ratio is largely independent of the overall efficiencies for particle tagging and π^0 reconstruction. The residual efficiency correction due to differences in K/π tagging and π^0 momentum spectra was obtained by Monte Carlo. A value of the ratio of 0.025 ± 0.009 was obtained. Using the value of $\text{BR}(\tau \rightarrow \rho^-\nu_\tau) = (22.4 \pm 1.5)\%$ measured by DELPHI [3], the result corresponds to $\text{BR}(\tau \rightarrow K^{*-}\nu_\tau) \times \text{BR}(K^{*-} \rightarrow K^-\pi^0) = (0.57 \pm 0.23)\%$.

Several sources of systematic errors were investigated. The most important ones are summarized in Table 3: Monte Carlo statistics, uncertainties in the efficiency of the kaon identification, asymmetry of the resolution function and uncertainties in the energy and efficiency for the π^0 reconstruction. There was also a small contribution from background arising from charged kaons plus neutrals giving invariant masses in the K^{*-} mass range. No correction was made for the contributions from $K^*\pi$ and K^*K decays. A systematic error of 10%, based on the measured branching ratios [5], was assigned.

7. Discussion and summary

Kaon production in single prong τ decays was studied using the particle identification capabilities of the DELPHI RICH detector. A data sample corresponding to 392 000 hadronic Z^0 events from 1992 was used. The uncertainties were dominated by statistics. The results are:

$$\text{BR}(\tau \rightarrow K\nu_\tau) = (0.85 \pm 0.18)\%$$

$$\text{BR}(\tau \rightarrow K\nu_\tau \geq 0 \text{ neutrals}) = (1.54 \pm 0.24)\%$$

$$\text{BR}(\tau \rightarrow K\nu_\tau \geq 1 \text{ neutrals}) = (0.69 \pm 0.25)\%$$

The measurement of the branching ratio for inclusive kaon production in single prong τ decays is consistent with the Particle Data Group average [5] of $(1.68 \pm 0.24)\%$ and has a similar accuracy. The present determination of the non-exclusive branching ratio is more precise than the earlier measurement [7] of $1.2_{-0.6}^{+0.5}$. The main contribution to this channel comes from the decay $\tau \rightarrow K^{*-}\nu_\tau \geq 0$ neutrals. The exclusive τ decay into K^{*-} was studied in the channel $K^{*-} \rightarrow K^-\pi^0$. The result $\text{BR}(\tau \rightarrow K^{*-}\nu_\tau) \times \text{BR}(K^{*-} \rightarrow K^-\pi^0) = (0.57 \pm 0.23)\%$ was obtained.

The $\tau \rightarrow K\nu_\tau$ exclusive branching ratio has been measured earlier by DELCO at PEP [8] and MARK2 at SPEAR [9] to be $(0.67 \pm 0.23)\%$ [5]. The present result substantially reduces the uncertainty. In the Standard Model, the decays $\tau \rightarrow K\nu_\tau$ and $K \rightarrow \mu\nu_\mu$ proceed by the same mechanism and the width $\Gamma(\tau \rightarrow K\nu_\tau)$ computed from the K decay involves only kinematical factors. The result of this calculation predicts a branching ratio of $(0.73 \pm 0.01)\%$ where the error reflects the experimental uncertainties on the τ lifetime, the K lifetime, the branching ratio of the decay $K \rightarrow \mu\nu_\mu$ and the radiative corrections [10]. The present result is in excellent agreement with the theoretical prediction.

A similar study using a statistical identification of kaons from their specific energy loss has been recently published by the Aleph collaboration [11].

Acknowledgements

We are greatly indebted to our technical collaborators and to the funding agencies for their support in building and operating the DELPHI detector, and to

the members of the CERN-SL Division for the excellent performance of the LEP collider.

References

- [1] DELPHI Collab, P Aarnio et al., Nucl Instr and Meth A 303 (1991) 233
- [2] E Anassontzis et al, Nucl Instr. and Meth A 323 (1992) 351
- [3] DELPHI Collab, P. Abreu et al., Z. Phys C 55 (1992) 555
- [4] S. Jadach, B FL. Ward and Z Was, Comput Phys Commun.66 (1991) 276.
- [5] Review of Particle Properties, Phys Rev. Lett D 45 (1992).
- [6] T. Sjostrand, "PYTHIA 5.6 JETSET 7.3 Physics and Manual", preprint CERN-TH 6488/92 (1992)
- [7] TPC Collab, H Aihara et al, Phys. Rev. D 35 (1987) 1553
- [8] DELCO Collab, G B Mills et al, Phys. Rev Lett. 52 (1984) 1944.
- [9] MARK2 Collab., C. Blocker et al, Phys Rev Lett 48 (1982) 1586.
- [10] R Decker and M. Finkemeier, University of Karlsruhe preprint TTP94-5, 1994, WJ Marciano and A Sirlin, Phys Rev. Lett. 71 (1993) 3629
- [11] ALEPH Collab., D Buskulic et al, CERN-PPE/94-58 (1994).